HHS Public Access

Author manuscript

Nat Neurosci. Author manuscript; available in PMC 2012 July 01.

Published in final edited form as:

Nat Neurosci. ; 15(1): 70–80. doi:10.1038/nn.3000.

TRPA1 channels regulate astrocyte resting calcium levels and inhibitory synapse efficacy via GAT-3

Eiji Shigetomi[1,*], **Xiaoping Tong**[1,*], **Kelvin Y. Kwan**[3], **David P. Corey**[3], and **Baljit S. Khakh**[1,2,Ψ]

[1]Department of Physiology, David Geffen School of Medicine, University of California Los Angeles, Los Angeles USA CA 90095-1751

[2]Department of Neurobiology, David Geffen School of Medicine, University of California Los Angeles, Los Angeles USA CA 90095-1751

[3]Howard Hughes Medical Institute, Harvard Medical School, Neurobiology, Goldenson 444, 220 Longwood Ave, Boston, MA 02115

Abstract

Astrocytes contribute to the formation and function of synapses and are found throughout the brain where they display intracellular store mediated Ca^{2+} signals. Here, using a membrane tethered genetically encoded calcium indicator (Lck-GCaMP3), we report the serendipitous discovery of a novel Ca^{2+} signal in rat hippocampal astrocyte-neuron co-cultures. We found that TRPA1 channel mediated Ca^{2+} fluxes give rise to frequent and highly localised near membrane "spotty" Ca^{2+} microdomains that contribute significantly to resting Ca^{2+} levels of astrocytes. Mechanistic evaluations in brain slices show that decreasing astrocyte resting Ca^{2+} levels mediated by TRPA1 channels decreased interneuron inhibitory synapse efficacy by reducing GABA transport via GAT-3, thus elevating extracellular GABA levels. Our data indicate how a novel transmembrane Ca^{2+} source (TRPA1) targets a transporter (GAT-3) in astrocytes to regulate inhibitory synapses.

Important progress has been made over the last century in understanding the roles of astrocytes in the brain[1,2]. These ubiquitous cells buffer potassium ions, contribute to injury and disease, control blood flow, contribute to synapse formation, respond to neuronal excitation and regulate neurons. Additionally, there is recent evidence both for[3] and against[4] a role of astrocyte Ca^{2+} signals in synaptic function and plasticity.

[Ψ]Correspondence to BSK at Department of Physiology, David Geffen School of Medicine, University of California, Los Angeles, 10833 Le Conte Avenue, 53-263 CHS, Los Angeles, CA 90095-1751, Fax: 310 206 5661, Tel : 310 825 6258, bkhakh@mednet.ucla.edu.

[*]authors with equal contributions to experiments (ES and XT)

Author contributions: ES and XT carried out the experiments with guidance from BSK. BSK directed the research project. KK and DPC generated the knockout mice. BSK, ES and XT generated the figures. BSK wrote the paper and all authors contributed to the final version.

Past studies on astrocyte functions in neuronal circuits have mainly explored the signalling roles of Ca^{2+} signals that originate from intracellular stores. The complete understanding of store mediated Ca^{2+} signals is an important goal for the field and is vital to our understanding of astrocytes because they express many Ca^{2+}-mobilising G-protein coupled receptors. However, the existence and/or functions of other astrocyte Ca^{2+} signals has received little attention, although pioneering studies show that astrocytes express ion channels and transporters[5]. An exception is recent work on the role of TRPC channels in gliomas[6].

In order to study near membrane Ca^{2+} signals in detail we recently refined a membrane targeted genetically encoded Ca^{2+} indicator (GECI)[7,8] called Lck-GCaMP3 that increases in fluorescence when near membrane Ca^{2+} levels are elevated in astrocytes[9,10]. Using this GECI, that is based on the significantly improved cytosolic GCaMP3[7,8] fused to a membrane tethering domain (Lck)[9,10], we report the serendipitous discovery of a novel Ca^{2+} signal mediated by TRPA1 channels in astrocyte-neuron co-cultures, its role in setting resting Ca^{2+} levels and how this regulates inhibitory synapse efficacy in the hippocampus via astrocyte GAT-3.

Results

Discovery and properties of spotty Ca^{2+} signals

We expressed Lck-GCaMP3 in mixed cultures of postnatal rat hippocampal neurons and astrocytes *in vitro* (herein called co-cultures) and observed spontaneously occurring “spotty” Ca^{2+} signals in astrocytes. These unexpected signals appeared as flashes (Supplementary Video 1; Fig. 1). The bright spots (regions of interest 1 to 8 in Fig. 1a), occurred repeatedly at the same site (Fig. 1b–c; 0.56 ± 0.02 events/min, n = 696 sites from 54 cells), lasted seconds ($t_{0.5}$ = 3.7 ± 0.1 s, n = 2735 events) and displayed full width half maxima (FWHM) of ~5 μm (Fig. 1d), and were thus microdomains smaller than a typical astrocyte[11]. On average, spotty Ca^{2+} signals increased Lck-GCaMP3 fluorescence by 150% (dF/F = 1.5 ± 0.02, n = 3021 events) corresponding to a change in free cytosolic Ca^{2+} concentration[9,10] of ~0.3 to ~0.5 μM[1].

Spotty Ca^{2+} signals were also observed in the cytosol with Fluo-4 using total internal reflection fluorescence (TIRF) microscopy[12] (Fig. 1e–f), indicating that they were not dependent on the Lck-GCaMP3 reporter. Moreover, with the benefit of dual emission imaging, some spotty Ca^{2+} signals could be detected simultaneously with cytosolic Fura Red, albeit unreliably (<50% of signals) and with poor signal-to-noise (Supplementary Fig. 1) providing a first clue that they represent Ca^{2+} signals that are maximal in the plane of the plasma membrane and thus optimally detected using Lck-GCaMP3. We focussed on using Lck-GCaMP3, but verified key experiments using TIRF microscopy and Fluo-4 as indicated. Spotty Ca^{2+} signals required Ca^{2+} entry across the plasma membrane, but were independent of Ca^{2+} release from intracellular stores (Fig. 1g, Supplementary Video 2; Supplementary Fig. 2a–c).

Evidence that TRPA1 channels mediate spotty Ca^{2+}signals

We initially used a pharmacological approach to identify the proteins mediating spotty Ca^{2+} signals and generated largely negative data, ruling out many ion channels (Supplementary Table 1 and Supplementary Fig. 2c). However, we found that Gd^{3+} and La^{3+} dramatically reduced spotty Ca^{2+} signals (Supplementary Fig. 2c and Supplementary Table 1), thus drawing attention to TRP channels[13]. Of the TRP channel blockers tested, HC 030031 (40 μM) almost completely and reversibly abolished spotty Ca^{2+} signals (~99% block; Fig. 2a; Supplementary Fig. 2d, e; Supplementary Video 3), but did not decrease basal fluorescence of Lck-GCaMP3, which reflects fluorescence in the absence of Ca^{2+} as suggested by Fig. 1g and our previous characterization studies[9,10]. HC 030031 is a recently discovered and selective TRPA1 channel blocker[14]. In keeping with its specificity[14] HC 030031 did not affect intracellular store mediated Ca^{2+} responses mediated by P2Y receptors in co-cultures (< 0.5% change; Supplementary Table 2, Supplementary Fig. 2c). Moreover, HC 030031 did not affect Ca^{2+} responses triggered by glutamate (1 mM; dF/F values were 3.3 ± 0.4 and 3.5 ± 0.4 for control (n = 17) and in HC 030031 (n = 23)). Interestingly, we observed increased spotty Ca^{2+} signals on washout of HC 030031 (Fig. 2a, b), suggesting that TRPA1 channels may become sensitized during blockade by HC 030031.

To explore the roles of TRPA1 channels in mediating spotty Ca^{2+} signals, we used a control siRNA that did not target any gene product and three separate siRNAs against distinct targets in TRPA1 (Supplementary Table 1). Spotty Ca^{2+} signals were observed in ~40% of astrocytes with control siRNA in our co-cultures, but three siRNAs with distinct targets (siRNAs 1–3) against TRPA1 significantly decreased the number of astrocytes showing spotty Ca^{2+} signals ($p < 0.01$; Fig. 2c,d, Supplementary Videos 4 and 5; Supplementary Fig. 2f–h). These same siRNAs did not affect P2Y receptor medi ated Ca^{2+} signals in astrocytes due to intracellular Ca^{2+} release (Fig. 2e; $p > 0.05$).

Low concentrations of the TRPA1 agonist allyl isothiocyanate (AITC; 1 μM)[15,16], which increases channel open probability, increased the numbers of spotty Ca^{2+} signals in co-cultures (Fig. 2f and Supplementary Video 6; 119 sites recorded from 8 cells) and this effect was abolished with TRPA1 siRNA (Fig. 2g; 4 sites recorded from 14 cells). Over expression of recombinant mTRPA1 channels also caused a large increase in the number of spotty Ca^{2+} signals in co-cultures (n = 12; $p < 0.00001$; Supplementary Fig. 3a,b; Supplementary Videos 7 and 8) and recombinant TRPA1 recapitulated spotty Ca^{2+} signals and AITC-evoked Ca^{2+} elevations in HEK-293 (Supplementary Fig. 3c–e), indicating that TRPA1 channels have sufficiently open fractions[17] to cause spotty Ca^{2+} signals.

We also used Fluo-4 based imaging and found that the TRPA1 agonist AITC elevated astrocyte global Ca^{2+} levels (Fig. 2h) and that this effect was abolished in co-cultures transfected with three siRNAs against TRPA1 (Fig. 2i) and by HC 030031 (control dF/F was 2.2 ± 0.6 (n = 22), whereas in the presence of HC 030031 dF/F was 0.1 ± 0.1 (n = 20); $p < 0.01$). Global astrocyte Ca^{2+} elevations mediated by P2Y receptors were not affected by these siRNAs (Supplementary Fig. 4), which also did not affect glutamate-evoked Ca^{2+} signals in neurons (control dF/F was 4.7 ± 0.5 whereas in cells with siRNA #1 the dF/F was 5.0 ± 0.6; n = 9).

Findings on TRPA1 channel expression in astrocytes

A transcriptome database shows that astrocytes do not express significant TRPA1 mRNAs[18]. We sought to evaluate the presence of TRPA1 proteins in astrocytes using immunocytochemistry, but were stymied by staining not different from background (unpublished observations). This could reflect the poor quality of the antibodies for immunostaining, or the fact that TRPA1 channels function at expression levels below the reach of immunocytochemistry, as recently demonstrated[19]. Instead we used a functional and Western blot approach.

We made whole-cell recordings from astrocytes from co-cultures and recorded AITC-evoked currents (−194 ± 70 pA at −60 mV; n = 5, 100 μM AITC), which displayed current-voltage relationships that reversed direction at +4.1 ± 1.8 mV, and were similar to AITC-evoked currents mediated by recombinant mTRPA1 channels (Supplementary Fig. 5a; n = 14, 100 μM AITC). Moreover, the AITC-evoked currents mediated by recombinant mTRPA1 channels were significantly reduced ~70% by TRPA1 siRNA that blocked spotty Ca^{2+} signals in co-cultures (Supplementary Fig. 5a). Consistent with the HEK-293 cell data, AITC-evoked currents in astrocytes were also reduced ~60% by siRNAs, but K^+ currents were unaffected (Supplementary Fig. 5b,c). We also performed Western blot analysis using an antibody tested against recombinant rTRPA1[20] (Supplementary Fig. 5d), detected a 130 kDa band indicative of TRPA1 and found that its intensity was decreased significantly by the siRNA against TRPA1 in the co-cultures (Supplementary Fig. 5e).

Spotty Ca^{2+} signals and their relation to neurons

The experiments described in Figs. 1–2 employed co-cultures, so we explored the possibility that spotty Ca^{2+} signals may require neurons. Neurons were identified by their round soma and dendrites, whereas astrocytes were identified as relatively flat cells with no dendrites. We found spotty Ca^{2+} signals were not affected by blocking action potentials or by ATP and glutamate receptor antagonists providing evidence against action potential-dependent ATP and glutamate release (Supplementary Fig. 6). We also readily observed spotty Ca^{2+} signals, AITC-evoked Ca^{2+} signals (that were blocked by HC 030031) and TRPA1 proteins in astrocyte enriched cultures (Supplementary Fig. 7).

We found that several previously reported agonists[21] of TRPA1 channels such as AITC (20 μM; n = 62), allicin (10 μM; n = 37), acrolein (20 μM; n = 27), N-methylmaleimide (NMM; 50 μM; n = 22), formaldehyde (FA; 0.01%; n = 36), nicotine (1 mM; n = 26) and menthol (30 μM; n = 34) all elevated global Ca^{2+} levels in astrocytes but had little or no effects on neurons in our co-cultures (Supplementary Fig. 8). However, glutamate (1 mM; n = 11 neurons; n = 25 astrocytes) elevated Ca^{2+} levels in both cell types (Supplementary Fig. 8).

We imaged Fluo-4 loaded astrocytes in the stratum radiatum in the CA1 region of rat hippocampal slices[22] and found that 19 of 50 astrocytes showed Ca^{2+} increases during applications of AITC (100 μM; Fig. 2j,k). AITC-evoked Ca^{2+} signals were significantly reduced by ~80% by HC 030031 (80 μM, Fig. 2k; $p < 0.05$), although some cells still showed responses (Fig. 2j,k), and consistent with their near membrane nature, AITC-evoked Ca^{2+} transients (n = 19) were smaller than P2Y receptor-mediated global Ca^{2+} signals (100

μM; Fig. 2k, n = 21) but were comparable in amplitude to mGluR-mediated Ca^{2+} global calcium signals evoked by DHPG (10 μM; Fig. 2k, n = 33). In contrast to their actions at astrocytes, neither AITC nor HC 030031 affected the membrane properties of pyramidal neurons in hippocampal slices (Supplementary Table. 3).

TRPA1 contributes to astrocyte resting calcium levels

To explore if spotty Ca^{2+} signals contributed to the resting Ca^{2+} levels of astrocytes we applied HC 030031 (40 μM) to co-cultures. We found that HC 030031 blocked spontaneous Ca^{2+} signals measured in astrocytes, but also that HC 030031 markedly reduced basal Ca^{2+} levels as measured by Fluo-4 (Fig. 3a; n = 13). In contrast HC 030031 had no effect on basal Ca^{2+} levels of neurons (Fig. 3b; n = 9). With ratiometric Fura-2 based imaging we found that HC 030031 significantly reduced basal Ca^{2+} levels from ~120 nM to ~50 nM in astrocytes but not neurons ($p < 0.01$; Fig. 3c; n = 10, Fig. 3d; n = 7). These data provide evidence that spontaneous openings of TRPA1 channels, which are seen as spotty Ca^{2+} signals with Lck-GCaMP3 in co-cultures (Figs. 1–2), contribute to resting Ca^{2+} levels in astrocytes (Fig. 3).

In keeping with the spontaneous nature of spotty Ca^{2+} signals in co-cultures (Figs. 1–2), in 43% of astrocytes in hippocampal slices, HC 030031 significantly reduced basal Fluo-4 fluorescence from resting levels that are thought to be ~100 nM[23] (Fig. 3e, n = 30 of 69 cells; example astrocyte images in Supplementary Fig. 9). However, HC 030031 did not affect spontaneous global Ca^{2+} elevations in the somata of astrocytes in rat brain slices ($p = 0.450$; control $dF/F = 0.22 \pm 0.03$, n = 24; in HC 030031 $dF/F = 0.18 \pm 0.04$, n = 18), that are known to originate from store mediated Ca^{2+} release[24].

We explored HC 030031-evoked decreases in basal Ca^{2+} levels in *TRPA1*$^{-/-}$ mice[25] in relation to parallel experiments with wild type mice (Fig. 3f,g). We found that the ability of HC 030031 to reduce resting Ca^{2+} levels of astrocytes was significantly reduced by ~75% in hippocampal slices from *TRPA1*$^{-/-}$ mice (although a ~25% component persisted). This can be seen from the cumulative probability plot of HC 030031 evoked dF/F in astrocytes from wild type and *TRPA1*$^{-/-}$ mice (Fig. 3f) as well as from average data (Fig. 3g; n = 127 and 66 astrocytes from 3 *TRPA1*$^{-/-}$and 3 wild type mice). Control ADPβS-evoked calcium elevations were equivalent in astrocytes from wild type and *TRPA1*$^{-/-}$ mice (Fig. 3g).

Reducing astrocyte Ca^{2+} levels decreases mIPSC amplitudes

Relatively little is known about inhibitory synapse regulation by astrocytes. We explored if astrocyte Ca^{2+} levels affect fast GABAergic inhibitory synapses onto interneurons and pyramidal neurons in the hippocampus of mice. We made whole-cell patch-clamp recordings from astrocytes and CA1 pyramidal neurons as well from astrocytes and stratum radiatum interneurons in hippocampal slices (Fig. 4a,b). The astrocyte intracellular solution contained the Ca^{2+} chelator BAPTA (13 mM) to buffer Ca^{2+} to nanomolar levels[26] in a syncytium of coupled astrocytes (Fig. 4).

We recorded mIPSCs (in 1 μM TTX) to sample ongoing transmission from a large number of synapses in an afferent input independent manner[27,28] because this has the potential to

reveal if all synapses onto a given neuron are modified equivalently[27]. We monitored mIPSCs onto "control" neurons in relation to those recorded from neurons located within 100 μm of astrocytes dialysed with BAPTA (Fig. 4c–f). We found no effect of astrocyte dialysis with BAPTA on mIPSC amplitude or frequency arriving onto pyramidal neurons (Fig. 4c,e). Control amplitudes and frequency were −36 ± 2 pA and 2.2 ± 0.2 Hz (n = 19), whereas mIPSC amplitude and frequency from pyramidal neurons located near astrocytes dialyzed with BAPTA were −36 ± 5 pA and 1.9 ± 0.3 Hz (n = 6; Fig. 4c,e). In contrast, when we monitored mIPSCs onto interneurons we detected a significant ~ 30% decrease in their amplitude ($p < 0.01$), whereas their frequency ($p > 0.05$) was unaffected (Fig. 4d,f). This was apparent in every interneuron we recorded. Data shown in Fig. 4d,f were gathered over a six month period: control amplitudes and frequencies were −36 ± 1 pA and 1.9 ± 0.2 Hz (n = 66) whereas for interneurons located near astrocytes dialyzed with BAPTA they were −25 ± 1 pA and 1.5 ± 0.2 Hz (n = 40; Fig. 4f).

The effect of BAPTA required ~20 min of astrocyte dialysis (Supplementary Fig. 10a), by which time 57 ± 6 of the surrounding astrocytes were dialyzed (n = 5). Astrocyte BAPTA dialysis did not affect mIPSC kinetics (Supplementary Fig. 10b), suggesting fewer channels opened during mIPSCs[28]. We found that in the majority of cases (6/8) BAPTA decreased mIPSC amplitudes by a multiplicative factor[27] of 0.73 ± 0.05 (n = 6; Supplementary Fig. 10c,d). Directly dialyzing interneurons with 13 mM BAPTA did not change mIPSCs (n = 14; Supplementary Fig. 11a,b).

"Ca^{2+} clamping" of astrocytes

The resting free Ca^{2+} concentration of astrocytes is ~ 100 nM[23]: we clamped astrocyte Ca^{2+} at about 35, 120, 310 and 500 nM using BAPTA. *First*, we found that clamping astrocyte Ca^{2+} to ~120 nM produced no effect on interneuron mIPSC amplitudes (Fig. 4g), showing that patching and dialyzing astrocytes *per se* does not reduce mIPSCs and that clamping astrocyte Ca^{2+} to near resting levels is without effect. *Second*, we found that clamping astrocyte Ca^{2+} levels to ~35 nM significantly reduced mIPSCs onto interneurons by ~30% (Fig. 4h). *Third*, we found that increasing astrocyte Ca^{2+} levels to ~310 and 500 nM produced no effect in mIPSCs onto interneurons (Fig. 4i). We do not interpret the Ca^{2+} concentrations precisely, but take these data to generally indicate that reduced rather than elevated astrocyte Ca^{2+} levels are important for the regulation of interneuron mIPSC amplitudes. As expected from Fig 4a–f, the frequencies of mIPSCs were not altered by clamping astrocyte Ca^{2+} concentrations to 35, 120, 310 or 500 nM (Supplementary Fig. 11c–f).

Ca^{2+} buffers display characteristic "length constants"[26] over which they can effectively clamp Ca^{2+}. BAPTA is a fast Ca^{2+} buffer suited to clamp Ca^{2+} close to its source. We also clamped astrocyte Ca^{2+} to ~ 35 nM with the slower buffer EGTA, which cannot effectively clamp Ca^{2+} close to its source. We found that clamping astrocyte Ca^{2+} levels to 35 nM with EGTA did not alter interneuron mIPSC amplitudes (Fig. 4h), indicating that Ca^{2+} acts locally.

BAPTA occludes the effect of blocking TRPA1 on mIPSCs

Since TRPA1 channels contribute to resting astrocyte Ca^{2+} levels (Fig 3) we explored if TRPA1 blockade affected mIPSCs. HC 030031 (40 μM), did not affect either the resting or active membrane properties of interneurons or pyramidal neurons (Supplementary Fig. 12; Supplementary Table 3). We recorded mIPSCs from pyramidal neurons before and during HC 030031 and found that TRPA1 blockade did not change their amplitude (Fig. 5a; from −33 ± 2 to −33 ± 3 pA; n = 8) or frequency (1.1 ± 0.2 *versus* 1.0 ± 0.2 Hz; n = 8). This result is consistent with Fig 4 and serves as a control by showing that HC 030031 does not block $GABA_A$ channels. Moreover, in a separate set of experiments the non-specific TRPA1 blocker Gd^{3+} (100 μM) also did not affect mIPSCs onto pyramidal neurons (control −28 ± 3 pA, 4 ± 0.5 Hz and −27 ± 4 pA, 4 ± 0.6 Hz in Gd^{3+}; n = 5).

In contrast to our observations with pyramidal neurons, HC 030031 reduced the amplitude of mIPSCs onto interneurons by ~20% (Fig. 5b; from −37 ± 2 to −30 ± 2 pA; n = 11), without changing their frequency relative to control (0.1% DMSO; Fig. 5c–d). The effect of HC 030031 on interneuron mIPSCs took >8 min (Fig. 5c) and was mimicked by Gd^{3+}, which is a non-selective TRPA1 blocker and also by removing Ca^{2+} from the extracellular buffer. Neither Gd^{3+} nor Ca^{2+} free affected mIPSC frequency relative to vehicle controls (Fig. 5d).

Thus blocking TRPA1 channels mimics the effect of astrocyte BAPTA dialysis on interneuron mIPSCs (Fig. 4, Fig. 5b). To explore this further we dialyzed astrocytes with 13 mM BAPTA for ~ 20 mins and then applied HC 030031 (Fig. 5e). Our reasoning was that if TRPA1 channels are the source of Ca^{2+} that is buffered by BAPTA (Fig. 4), the effect of HC 030031 should be abolished with prior astrocyte dialysis with BAPTA. Exactly this was observed: for these experiments BAPTA reduced mIPSC amplitudes as expected (Supplementary Fig. 13a,b), but prevented any further effect of HC 030031 (Fig. 5e). These experiments also show that HC 030031 acts via astrocytes, because BAPTA was dialyzed only into astrocytes.

Interneuron tonic inhibition by astrocyte BAPTA dialysis

We applied bicuculline and confirmed that mIPSCs were due to $GABA_A$ channels in interneurons (Fig. 6a). During these experiments we found that bicuculline (20 μM) or SR95531 (100 μM) application evoked outward currents in interneurons that were located near BAPTA dialyzed astrocytes (Fig. 6a; n = 26 & 17). The existence of these tonic GABA currents[29] provides evidence that extracellular GABA levels were elevated after astrocytes had been dialyzed with BAPTA and suggests that phasic IPSCs may have been reduced (Figs. 4–5) because of $GABA_A$ receptor desensitization[28]. Consistent with this we found that currents evoked by 30 μM GABA puffs onto interneuron somata (Fig. 6b; n = 8) and evoked IPSCs (Supplementary Fig 13c) were also reduced in interneurons near astrocytes dialyzed with BAPTA. However, GABA-evoked currents were not affected when interneurons were directly dialyzed with BAPTA (Fig. 6b; n = 10).

Bergmann glia express GABA permeable bestrophin-1 channels, which lead to the tonic efflux of GABA from glia to sustain tonic $GABA_A$ receptor mediated inhibition in the

cerebellum[30]. If bestrophin-1 channels are involved in the responses described herein one would expect that bestrophin-1 channels may mediate the effects observed by astrocyte dialysis with BAPTA and HC 030031. In contrast we found that blocking bestrophin-1 channels had no effect on inhibitory synapses in the hippocampus (mIPSC amplitudes were −32 ± 4 pA in control *versus* −31 ± 4 pA in the presence of 100 μM NPPB, the bestrophin-1 blocker; n = 8).

Role of astrocyte GAT-3 GABA transporters

Past work shows that ambient GABA, due to neuronal GABA transporter GAT-1 inhibition, can reduce the amplitude of mIPSCs onto pyramidal neurons, most likely by increasing $GABA_A$ receptors in desensitized states from which they recover slowly[28]. Of the four known GABA transporters, GAT-1 and GAT-3 are widely expressed in brain including the hippocampus[31] and we hypothesized they may be involved in reduced mIPSCs and enhanced tonic currents as a result of astrocyte BAPTA dialysis (Fig. 4). We performed immunohistochemistry (IHC) to determine if either GAT-1 or GAT-3 were expressed in the stratum radiatum region of the hippocampus (Supplementary Fig. 14). Consistent with past work[32], we found robust expression of GAT-1 within punctate spots that did not colocalize with the astrocyte marker GFAP (Supplementary Fig. 14; n = 4). In contrast, we found that GAT-3 was expressed in astrocytes and colocalized with GFAP (Fig. 6c; Supplementary Fig. 14b; n = 5).

If the decrease in interneuron mIPSC amplitudes (caused by block of TRPA1 and astrocyte BAPTA) is due to GABA transport regulation, we would expect that blocking GABA transporters would also produce a similar effect. To test this we bath applied the broad spectrum GAT blocker nipecotic acid (NA; 100 μM) and found that the mean mIPSC amplitude was decreased ($p < 0.01$ n = 12) in 11/12 interneurons whereas the frequency was not affected (Fig. 6d). The effect of NA was mimicked by bath application of the GAT-3 specific blocker β-alanine (100 μM), but not by the GAT-1 and GAT-2 blockers NO-711 (10 μM) or hypotaurine (100 μM), respectively (Fig. 6d). We also performed a specific set of experiments with the GAT-3 blocker SNAP-5114 and found that it decreased mIPSCs from −29 ± 2 pA in control to −22 ± 2 pA (the frequency was unchanged at 1 ± 0.2 Hz, n = 6). Thus blocking GAT-3 produces a similar effect as that observed by dialyzing astrocytes with BAPTA or by blocking TRPA1 channels.

Next we investigated whether the effect observed by blocking GAT-3 (Fig. 6d,e) was occluded by prior dialysis of astrocytes with BAPTA (13 mM) or treatment with HC 030031 (40 μM). In both cases we found that astrocyte BAPTA dialysis and HC 030031 applications reduced interneuron mIPSC amplitudes and this occluded the inhibition observed by blocking GAT-3 with β-alanine (Fig. 6f,g). This suggests that reduced astrocyte intracellular Ca^{2+} levels, as a consequence of blocking TRPA1 channels or BAPTA dialysis, results in altered GAT-3 function because the effects of these perturbations were mutually occlusive.

Astrocyte Ca^{2+} regulates GAT-3 functional expression

Past work shows that GAT-1 surface expression is regulated by dynamin-dependent endocytosis[33,34]. In view of these findings, we set out to explore how astrocyte dialysis with

BAPTA may affect GAT-3 expression using combined patch-clamp recording and immunostaining. For these experiments we included Alexa-488 in the pipette solution and also added 13 mM BAPTA for specific experiments. After the recording session we processed the slices for GAT-3 immunostaining and determined if there were differences in GAT-3 expression in cells that had been dialyzed with BAPTA.

For astrocytes dialyzed with Alexa-488 (without BAPTA) we could easily identify the patched cell and measure GAT-3 expression, which colocalized with Alexa-488 (Fig. 7a; arrows). Moreover, from the surrounding slice we could also measure GAT-3 staining in coupled astrocytes that were dialyzed with Alexa-488 as well as in non coupled astrocytes that were not dialyzed with Alexa-488 (Fig. 7b). Of note, the GAT-3 staining was similar for the patched, coupled and non coupled astrocytes when the pipette solution contained only Alexa-488 (Fig. 7b), indicating that patching astrocytes does not lead to any measureable change in GAT-3 expression.

For astrocytes dialyzed with Alexa-488 and BAPTA (13 mM) we could also identify the patched cell and measure GAT-3 expression, but in this case GAT-3 signal was reduced by ~ 60% (open arrows in Fig. 7a,b). Moreover, GAT-3 staining in coupled astrocytes that were dialyzed with Alexa-488 and BAPTA was also reduced by ~ 40%, whereas it was not affected in non coupled astrocytes (Fig. 7b). We interpret this result to indicate that dialyzing astrocytes with BAPTA leads to decreases in GAT-3 immunostaining. We next determined if dynamin-dependent endocytosis was involved in the ability of BAPTA to reduce GAT-3 staining because of past work with GAT-1[33,34]. To this end, we repeated the astrocyte BAPTA dialysis experiments with the dynamin-dependent endocytosis inhibitor dynasore (100 μM) in the bath[35]. We found that this molecule abolished the BAPTA mediated decrease in GAT-3 expression in patched and coupled astrocytes (Fig. 7a,b).

The preceding experiments suggest that astrocyte dialysis with BAPTA may lead to diminished inhibitory synaptic currents because of a decrease in functional GAT-3 expression (Fig. 7a,b). If both BAPTA and HC 030031 act via GAT-3, one would predict that dynasore pretreatment, which prevents the BAPTA mediated decrease in GAT-3 expression (Fig. 7a,b), would block the ability of astrocyte BAPTA dialysis and HC 030031 to cause a decrease in mIPSC amplitudes. Before investigating this we first determined if dynasore itself affected inhibitory synaptic responses, and found it did not (Fig. 7c). However, BAPTA- and HC 030031 induced depression of mIPSC amplitudes was prevented by prior blocking of endocytosis by dynasore (Fig. 7d,e). In contrast, dynasore did not affect the ability of β-alanine to reduce mIPSC amplitudes (Fig. 7f). This experiment thus serves as a control and argues against non specific effects of dynasore on GAT-3.

Studies with TRPA1$^{-/-}$ mice and elevation of astrocyte Ca^{2+}

Taken together the preceding experiments provide strong evidence that a transmembrane Ca^{2+} flux pathway mediated by TRPA1 channels regulates GAT-3 mediated GABA transport in astrocytes, which in turn regulates the amplitude of mIPSCs arriving onto interneurons. To further explore this mechanism we repeated the experiments with intracellular BAPTA dialysis (Fig. 4) and HC 030031 (Fig. 5) in *TRPA1*$^{-/-}$ deletion mice[25]. The ability of both BAPTA and HC 030031 to reduce mIPSCs onto interneuorns was

abolished in mice lacking TRPA1, but not in parallel wild type controls (Fig. 8). These data provide strong evidence that HC 030031 acts via TRPA1 and that astrocyte dialysis with BAPTA reduces resting Ca^{2+} levels that are the result of TRPA1 mediated fluxes because both these effects are reduced in *TRPA1*$^{-/-}$ mice.

We found no significant effect of AITC (100 μM) on either mIPSC amplitude or frequency (Supplementary Fig. 15). We also applied 30 μM ADPβS and 100 nM endothelin-1 (ET-1), which are agonists of astrocyte G-protein coupled P2Y1 and ET-1 receptors, respectively. Although ADPβS and ET-1 strongly elevated astrocyte Ca^{2+} levels[4,36], they failed to change the frequency or amplitude of interneuron mIPSCs (Supplementary Fig. 15). We interpret these data to indicate that elevating astrocyte Ca^{2+} levels through these approaches does not affect mIPSCs arriving onto interneurons.

Discussion

The main findings of the present study are that spotty Ca^{2+} signals can be imaged with Lck-GCaMP3 and that they are due to TRPA1 channels in co-cultures. These microdomains contribute significantly to resting Ca^{2+} levels *in vitro* in co-cultures and *in situ* in hippocampal slices. Moreover, TRPA1 mediated resting Ca^{2+} levels in astrocytes regulate GAT-3, which in turn leads to changes in $GABA_A$ receptor mediated inhibitory synapse efficacy onto interneurons. Overall, our data show a specific and strong effect on interneuron mIPSCs mediated by a "classical" house-keeping role of astrocytes, i.e. neurotransmitter transport. Together with insights on gliotransmission, these studies highlight the diversity of roles played by astrocytes in neuronal circuits.

TRPA1 in relation to past work

A transcriptome study shows no significant levels of TRPA1 mRNA in astrocytes[18]. The evidence to support functional roles for TRPA1 channels in our studies is tenfold. *First*, random, spotty Ca^{2+} signals displayed different durations and amplitudes suggesting a "Ca^{2+} permeable channel-like event". In accord, removal of extracellular Ca^{2+} abolished the spotty Ca^{2+} signals. *Second*, three distinct siRNAs targeting TRPA1 channels resulted in the loss of spotty Ca^{2+} signals in co-cultures. *Third*, spotty Ca^{2+} signals were blocked by a TRPA1 blocker HC 030031[14] and by general TRP blockers (La^{3+} and Gd^{3+}). *Fourth*, low concentrations of AITC, expected to increase the open probability of TRPA1, caused the appearance of spotty Ca^{2+} signals. *Fifth*, TRPA1 is defined by the broad range of agonists that can activate it: we found that all of the TRPA1 agonists tested also elevated Ca^{2+} in astrocytes in co-cultures. *Sixth*, of the known TRPA1 agonists AITC is considered the most selective and we found that its agonist action in astrocytes was blocked by siRNA and HC 030031 that also blocked spotty Ca^{2+} signals. *Seventh*, we found evidence for TRPA1 proteins in co-cultures using Western blot analysis: the band corresponding to TRPA1 was reduced by siRNA that also decreased spotty Ca^{2+} signals. *Eighth*, we found electrophysiological evidence for TRPA1 in astrocytes, with AITC-evoked currents displaying current-voltage relations similar to recombinant TRPA1. *Ninth*, expression of recombinant TRPA1 in co-cultures increased the frequency of spotty Ca^{2+} signals and reproduced them in HEK-293 cells. *Tenth*, we found that HC 030031 reduced resting global

Ca^{2+} levels of astrocytes *in situ* and that this effect was almost completely abolished in TRPA1 deletion mice.

We interpret the preceding ten findings to suggest that a population of astrocytes express functional TRPA1 channels and that these mediate significant Ca^{2+} signalling events, but our experiments do not rule out TRPA1 expression in neurons as suggested by Cahoy et al[18] at levels we could not functionally detect. What then explains differences between astrocyte TRPA1 mRNA distributions and function as studied here? Perhaps low levels of TRPA1 mRNA might have been missed in past expression analyses, but that these levels are sufficient to cause spotty Ca^{2+} signals. This possibility gains support from the fact that TRPA1 channels display properties that make them well suited to mediate Ca^{2+} signals. Thus, TRPA1 channels display high Ca^{2+} permeability with a fractional Ca^{2+} current of ~17%[37]. Additionally, TRPA1 channels undergo pore dilation[38] that increases their Ca^{2+} permeability[37]. Finally, Ca^{2+} itself activates TRPA1 channels[39,40], which may recruit and/or prolong channel opening mediated by small numbers of TRPA1 channels. Broadly speaking these findings are similar to recent findings with *Drosophila* body wall photoreceptors, which display significant Ca^{2+} signals with TRPA1 expression levels too low to detect by immunocytochemistry[19].

Spontaneous nature of spotty Ca^{2+} signals

We measured TRPA1 Ca^{2+} signals in co-cultures and slices in the absence of agonist activation. This is likely because TRPA1 displays significant open fractions at the whole-cell and single-channel level in the absence of ligand[17,41], a finding we verified in HEK-293 cells expressing recombinant TRPA1 indicating that spotty Ca^{2+} signals are most likely caused by spontaneous TRPA1 channel openings. Other TRP channels known to be expressed in astrocytes (e.g. the TRPC channels) require activation via second messengers or release of Ca^{2+} from intracellular stores[42–45]. As such they would not contribute to the spontaneous Ca^{2+} signals we have studied. Intriguingly, TRPA1 channels are multimodal receptors that are activated by several diverse stimuli[13]. Thus, we cannot formally exclude the possibility that astrocytes release or contain a native ligand(s) for TRPA1: this possibility merits further exploration. Such a hypothetical ligand would presumably also exist in HEK-293 cells (Supplementary Fig. 3).

We comment on our use of AITC to activate TRPA1 channels. Although AITC activates TRPA1, it also activates TRPV1[46]. However, the EC_{50} of AITC for TRPV1 is 3 mM whereas for TRPA1 it is 33 μM[16,46]. We also emphasise that the AITC-evoked responses reported in this study were reduced by TRPA1 specific siRNAs and by a TRPA1 antagonist. We also found that the TRPV1 agonist capsaicin (10 μM) did not increase Ca^{2+} levels, suggesting that TRPV1 was not functionally expressed in co-cultures.

Astrocyte resting Ca^{2+} levels and mIPSCs

We found that buffering astrocyte Ca^{2+} strongly reduced the efficacy of inhibitory synapses onto interneurons, but not pyramidal neurons. This implies a closer functional relationship between GAT-3 expressing astrocyte processes with interneurons than with pyramidal neurons, or that mIPSCs in pyramidal neurons are less susceptible to ambient GABA, a

possibility supported by recent work[47]. In relation to this, synaptic inhibition onto pyramidal neurons is reduced during reactive astrogliosis[48]. Insofar as we did not observe a similar effect, our data suggest that BAPTA dialysis does not trigger astrogliosis over ~30 minutes. Moreover, since BAPTA was dialyzed directly into astrocytes these experiments provide evidence that astrocyte Ca^{2+} levels impact inhibitory synapses onto interneurons.

By buffering astrocyte Ca^{2+} levels at different levels using BAPTA we found that reducing resting levels decreased interneuron inhibitory synapse efficacy. In contrast, clamping astrocyte Ca^{2+} at resting (~100 nM) or elevated levels (up to 0.5 μM) was without affect. For these experiments the concentration of BAPTA in each case was 13 mM and the only parameter that changed was the free concentration of Ca^{2+} ions. We observed clear and significant decreases in mIPSCs when astrocyte Ca^{2+} levels were reduced with the fast chelator BAPTA, but not when they were reduced to similar levels by EGTA. Considering the on rates (which differ ~170-fold) and affinity of EGTA and BAPTA for Ca^{2+} (~ 120 nM)[26], we estimate that the distance between Ca^{2+} source and effector is probably no more than ~ 250 nm[26], recalling recent work[27] revealing local astrocyte signaling.

Astrocyte TRPA1 channel regulate mIPSCs via GAT-3

Our data suggest that TRPA1 channels are the source of Ca^{2+} that regulates interneuron mIPSCs. The evidence is six fold. *First*, the TRPA1 antagonist HC 030031 mimics the effect of astrocyte BAPTA dialysis on interneuron mIPSCs. *Second*, HC 030031 reduces resting Ca^{2+} levels in astrocytes in co-cultures and *in situ. Third*, astrocyte BAPTA dialysis occludes the effect of HC 030031 on mIPSCs, providing strong evidence that HC 030031 acts via astrocytes because these are the only cells that were dialyzed. *Fourth*, the actions of HC 030031 and BAPTA dialysis are both abolished in *TRPA1*$^{-/-}$ mice, likely because once the source of Ca^{2+} is removed (TRPA1) there is little further effect of the antagonist or BAPTA. *Fifth*, HC 030031 had no detectable effect on the passive or active membrane properties of interneurons. *Sixth*, neither HC 030031 nor BAPTA dialysis affected inhibitory synapses onto pyramidal neurons, providing strong evidence that neither approach affects $GABA_A$ channels directly. Overall, the work with HC 030031, BAPTA and *TRPA1*$^{-/-}$ mice provides strong evidence that reducing Ca^{2+} levels below resting levels in astrocytes affect mIPSCs.

Our experiments show that astrocyte resting Ca^{2+} levels affect the functional expression of GAT-3 in astrocytes, which leads to elevated extracellular GABA levels and reduced interneuron mIPSCs. We measured a ~30% decrease in interneuron mIPSC amplitudes when GAT-3 was blocked, or when astrocyte Ca^{2+} levels were reduced by BAPTA dialysis or by application of HC 030031. In relation to this, low concentrations of GABA have been shown to decrease the amplitude of IPSCs by ~23–30%[28]. Our data suggest that astrocyte resting Ca^{2+} levels regulate the functional expression of GAT-3 on the plasma membrane, because blocking dynamin-dependent endocytosis occluded the effects mediated by astrocyte BAPTA dialysis and HC 030031 on mIPSCs. Past work has established that GAT-1 is dynamically regulated by endocytosis[34]. In future work it will be important to explore this possibility for GAT-3 with antibodies raised against its extracellular portions

when they become available and to directly study GAT-3 trafficking in astrocytes using methods pioneered for GAT-1[49].

Online methods

Measuring spotty Ca^{2+} signals

Briefly, we used an Olympus IX71 microscope equipped with an IXON EMCCD camera (Andor), epifluorescence condenser, control unit and Polychrome V monochromator (TILL photonics). We used an Olympus 60X 1.45 NA objective lens. Images were typically taken every second. Cultures were perfused with recording buffer (110 mM NaCl, 5.4 mM KCl, 1.8 mM $CaCl_2$, 0.8 mM $MgCl_2$, 10 mM D-glucose, 10 mM HEPES at pH 7.4 (adjusted with NaOH). The astrocytes expressed Lck-GCaMP3 to report near membrane Ca^{2+} signals. For calcium imaging with organic calcium indicator dyes, astrocytes were loaded with Fluo–4/AM (2.5 μM, Invitrogen) for 10 min or FuraRed (10 μM) for 2 hours. We used 0.05% Pluronic® F–127 20% solution in DMSO (Invitrogen) to facilitate loading of organic calcium indicators.

Hippocampal astrocyte-neuron co-cultures

Hippocampal cultures were prepared exactly as described by us[10,12].

Astrocyte only cultures

We used two *Sprague-Dawley* rat pups at P1–2 for each dissection. We used 12 pups in total for the experiments reported for these specific experiments reported in this paper. All procedures were approved by the UCLA Institutional Animal Care and Use Committee. Hippocampi were dissected in Petri dishes filled with ice-cold medium. The dissected hippocampi (in medium, on ice) were cut and then digested with 0.25% trypsin for 30 min at 37°C (Invitorgen). After the incubation, the pieces were washed with pre-warmed plating media consisting of DMEM (Invitrogen) with 10% fetal bovine serum (Hyclone) and 10% calf serum (Hyclone), 2 mM L-glutamine (Invitrogen), 100 U/ml penicillin/100 mg/ml streptomycin (Invitrogen) and 10 μg/ml epidermal growth factor (invitrogen) and triturated with flame-polished pipettes of progressively smaller bores; 60,000–80,000 cells (for 22 mm coverslips, VWR) were used for plating onto each coverslip. The coverslips were previously coated with poly-D-lysine (50 μg/ml; Sigma). One hour after plating the cells were fed with 2 ml of pre-warmed plating medium. Upon reaching con uence, cells were treated with 8 mM cytosine β-d-arabinofuranoside (Sigma) for 5–6 days to eliminate dividing cells.

Western blot analysis

Astrocytes were suspended in cell lysis buffer containing 20 mM HEPES, 100 mM NaCl, 1 mM DTT, 1% Triton X-100, and a protease inhibitor cocktail tablet (GE Healthcare). Typically 3–4 22mm coverslips with attached cells were used for each lysate. Cells were triturated with a 27-gauge syringe needle and incubated in the lysis buffer for 30 min at 4°C. This mixture was then centrifuged at 13,000 rpm for 30 min at 4°C: the soluble proteins in the supernatant were transferred into a clean tube. Equal amounts of proteins were loaded on 10% SDS-PAGE gels and transferred to nitrocellulose membrane (GE Healthcare). After transfer, membranes were blocked by incubation with PBS containing 0.05% Tween and 5%

dry milk for 2 h and incubated overnight with antibodies against TRPA1 proteins in PBS containing 5% milk at 4°C. The antibodies used were anti-TRPA1 (1 μg/ml; abcam). After washing three times for 10 min each in PBS/Tween, the membranes were incubated with anti–rabbit horseradish peroxidase secondary antibodies (1:5,000; Invitrogen) in PBS containing 5% milk for 1 h at room temperature. Membranes were washed three times for 10 min each in PBS/Tween, and the protein bands were imaged using ECL reagent (Thermo Fisher Scientific). Standard β actin controls (anti-β actin; 1:1,000; abcam) were included to ensure equal loading and to use for normalization of the TRPA1 band intensities.

TRPA$^{-/-}$ mice

The *TRPA1*$^{-/-}$ mice were available from previous work, which also describes in detail their generation and maintenance[25].

Transfection of co-cultures

We transfected plasmids (typically 600–1000 ng) into astrocytes at 4–6 days in culture with the Effectene transfection reagent (Qiagen) or Lipofectamine 2000 (invitorgen), following manufacture's instructions. For overexpression of mTRPA1, we transfected 600 ng of mTRPA1 plasmid and 300 ng of Lck-GCaMP3 plasmid. We transfected 100 ng of siRNA with Lipofectamine 2000. Before siRNA transfection, astrocytes were feed with fresh media without penicillin and streptomycin. When Fluo-4 was used for Ca^{2+} imaging, astrocytes were co-transfected with cytosolic mCherry plasmid (200 ng). When Lck-GCaMP3 was used for Ca^{2+} imaging, astrocytes were co-transfected with Lck-GCaMP3 plasmid (300 ng). Astrocytes were used 2–3 days after transfection. siRNAs against rat TPRA1 were obtained from Invitrogen: rTRPA1 siRNA #1–3. Negative control siRNA (Silencer ® Select Negative Control #1 siRNA) were obtained from Ambion. We chose to use the negative control siRNA instead of scrambled siRNA since the negative control siRNA has been widely used in the past. See Supplementary Table 1 for the sequences of siRNAs.

Patch-clamp recording from dissociated astrocytes

Astrocyte cultures were treated with 0.05% trypsin for 5 min at 37°C. After incubation with trypsin, 1 ml of fresh hippocampal medium was added to the cultures and collect cells in a 15 ml tube, which was centrifuged for 5 min at 800g. The media was removed and the cells resuspended in 300–500 μl of hippocampal buffer. 50 μl of these cells were plated onto 12 mm coverslips coated with poly-D-lysine in 12-well plates. 30 min later, 1 ml of fresh medium was added to cultures and kept in a humidified atmosphere of 95% air/5% CO_2 at 37 °C in a cell culture incubator. Astrocytes were treated with HC 030031 (40 μM) during the incubation. Recordings were done between 1–4 hours after the plating. The pipette solution comprised (in mM): KCl 154, EGTA 11 and HEPES 10 (pH 7.4). Whole-cell voltage clamp recordings were made with 3–6 MΩ borosilicate glass electrodes (WPI) using an Axopatch 700B controlled by a computer running pCLAMP 10.2 software via a Digidata 1322A interface (Axon Instruments). Data were filtered at 2 kHz and digitized at 5 kHz. The chamber housing the glass coverslip was perfused with extracellular buffer at a rate of 2–3 ml/min.

HEK-293 cell culture, transfection and electrophysiology

HEK-293 cells (obtained from ATCC) were maintained in 75 cm^2 cell culture flasks in DMEM/F12 media with Glutamax (Invitrogen) supplemented with 10% fetal bovine serum and penicillin/streptomycin. For transient expression in HEK-293 we used 0.5–1 μg plasmid cDNA and the Effectene transfection reagent (Qiagen) for each well of a 6 well plate. HEK-293 cells were used for recordings 24–48 h post transfection. The cells were gently mechanically dispersed and plated onto glass coverslips 2–12 hrs before use. The extracellular recording solution comprised (mM) NaCl 147, KCl 2, $MgCl_2$ 1, $CaCl_2$ 1, HEPES 10 and glucose 10 (pH 7.4), and the pipette solution (mM) KCl 154, EGTA 11 and HEPES 10 (pH 7.4). Whole-cell voltage clamp recordings were made with 3–5 MΩ borosilicate glass electrodes (WPI) using an Axopatch 200B controlled by a computer running pCLAMP 10.2 software via a Digidata 1322A interface (Axon Instruments).

Brain slice Ca^{2+} imaging

Briefly, young [postnatal day10 (P10)–P20] rats, C57BL/6J mice or *TRPA1*$^{-/-}$ mice were killed in accordance with institutional procedures. Coronal slices of hippocampus (300 μm) were cut (model 3000 Plus Vibratome) and submerged at room temperature in artificial CSF (aCSF) comprising the following (in mM): 126 NaCl, 2.5 KCl, 1.3 $MgCl_2$, 10 D-glucose,2.4 $CaCl_2$, 1.24 NaH_2PO_4, and 26 $NaHCO_3$ saturated with 95% O_2 and 5% CO_2 (flow rate = 2–3 ml/min). Brain slices were loaded at room temperature in the dark with5 μM Fluo-4/AM (Invitrogen) in aCSF for 60 min, then transferredto dye-free aCSF for at least 30 min before experimentation to allow for cleavage of the AM ester group. Live astrocytes were predominantly loaded with the fluorescent dye with these conditions. This was confirmed by simultaneous acquisition of infrared-differential interference contrast (IR-DIC) images of astrocytes in the same area. Slices wereimaged using an Olympus Fluoview 300 laser-scanning confocalmicroscope with a 300 mW argon laser, at < 2% power. Emittedgreen fluorescence was collected through a 515 long-pass filter. Fluoview software was used for image acquisition. Imaging were carried out in the presence of 6-cyano-2,3-dihydroxy-7-nitroquinoxaline (CNQX; 10 μM), DL-(−)-2-amino-5-phosphono-pentanoicacid (DL-AP5; 20 μM), bicuculline (10 μM), and TTX (1 μM). We added the same concentration of 0.1% DMSO in the control buffer, when we applied AITC or HC 030031.

Immunocytochemistry

Cultures were fixed with 1:1 solution of freshly prepared acetone and methanol for 5 min and then incubated for 7 min with PBS containing 0.25% TritonX-100. After blocking non-specific binding sites with 10% normal goat serum (NGS) for 30 min, cultures were incubated with primary antibodies in 2% NGS overnight at 4 °C. Primary antibodies used were polyclonal rabbit anti-GFAP antibody (1:10,000; DAKO), monoclonal mouse anti-GFAP antibody (1:400; Millipore), monoclonal mouse anti-S100b (1:1,000; Sigma), polyclonal chicken anti-MAP2 antibody (1:10,000; abcam) and polyclonal rabbit anti-Iba1 (1:1,000; Wako). After washing unbound antibody with PBS three times, cultures were incubated with secondary antibodies for 1 hour at RT. Secondary antibodies used were Alexa-488 conjugated goat anti-rabbit IgG (1:500; Invitrogen) Alexa546-conjugated goat anti-mouse IgG (1:500; Invitrogen) and Alexa546-conjugated goat anti-chicken IgG (1:500;

Invitrogen). To count number of cells, counterstaining of DAPI (1 μM; 30 min) was performed. Cultures were washed with PBS three times and then fluorescence images were taken using Leica SP2.

Brain slice preparation and electrophysiological recordings

Briefly, young P13 to P25 C57BL/6 mice, *TRPA1*$^{-/-}$ mice, or P12–15 *Sprague-Dawley* rat were killed in accordance with institutional procedures. Coronal slices of hippocampus (300 μm) were cut (model 3000 Plus; Vibratome, St. Louis, MO) and submerged at room temperature in artificial CSF (aCSF) comprising the following (in mM): 126 mM NaCl, 2.5 mM KCl, 1.3 mM $MgCl_2$, 2.4 mM $CaCl_2$, 1.24 mM NaH_2PO_4, 10 mM D-glucose, and 26 mM $NaHCO_3$, saturated with 95% O_2 and 5% CO_2. Experiments were performed at room temperature after the slices were allowed to recover for 1 hr after slicing. We identified interneurons and pyramidal neurons based on established criteria, including their anatomical location, morphology and electrophysiological properties as we have previously described. Whole-cell patch-clamp recordings (holding at −60 mV) were made from interneurons and pyramidal neurons with a pipette solution comprising (in mM): 130 KCl, 2 $MgCl_2$, 0.5 $CaCl_2$, 2.5 ATP, 0.3 GTP, 10 HEPES, 1 EGTA at pH 7.25. For recording of rat pyramidal neurons, experiments were performed with potassium gluconate, comprising the following(in mM): 120 K gluconate, 10 KCl, 1 $MgCl_2$, 0.03$CaCl_2$, 0.1 EGTA, 1 ATP, 0.2 GTP, 10 HEPES, and 4 glucose, pH7.25. The resistance of the pipettes was 4 – 6 MΩ. Cells were visualized with infrared optics on an upright microscope (BX71, Olympus). Miniature of inhibitory post-synaptic currents were recorded in the presence of 6-cyano-7-nitroquinoxaline- 2,3-dione (CNQX, 10 μM), DL-2-Amino-5-phosphonopentanoic acid (DL-AP5, 10 μM) to block AMPA/kainate and NMDA receptors and tetrodotoxin (TTX, 1 μM) to block the action potentials. Miniature of excitatory post-synaptic currents were recorded in the presence of bicuculline (10 μM) and TTX (1 μM) to block GABAergic synaptic currents. The pipette solution for whole-cell patch-clamp recordings from astrocyte comprised (in mM): 123 CsCl, 1 $MgSO_4$, 1 ATP-Mg, 0.2 GTP-Li, 10 HEPES (CsOH adjusted, pH = 7.24) at holding voltage of −80 mV.

Ca^{2+} clamping and imaging

In order to “clamp” astrocyte intracellular Ca^{2+} ion levels at different levels we used intracellular pipette solutions containing the fast Ca^{2+} chelator BAPTA. For these experiments the standard CsCl based intracellular solution with 13.2 mM BAPTA was used. To this we added $CaCl_2$ to reach free concentrations of Ca^{2+} 35, 120, 310 and 500 nM. The amount of $CaCl_2$ added to the intracellular solution was calculated using MaxChelator (http://www.stanford.edu/~cpatton/maxc.html). The 13.2 mM EGTA based intracellular solution with a free concentration of calcium ions at 35 nM was made similarly.

Immunohistochemistry

Fresh slices were fixed with 4% paraformaldehyde for 3 hours and gently washed with 0.1 M phosphate buffered saline (PBS) 3 times for 10 min each, followed by incubatation with 0.5% Triton X-100 for 45 min at 4°C. After blocking nonspecific binding sites with 10% normal goat serum for 2 hrs at 4°C, the slices were incubated with appropriate primary

antibody for 48 hour at 4°C. These were; rabbit polyclonal against GAT-1 (1:100, gift from Dr. Brecha at UCLA), rabbit polyclonal against GAT-3 (1:500, gift from Dr. Brecha UCLA) or chicken polyclonal to GFAP (1:500, Abcam). After washing unbound antibody with PBS three times, slices were incubated with conjugated goat anti-rabbit or goat anti-chicken IgG (1:800, Invitrogen) for 3 hrs at room temperature. Slices were washed with 0.1 M PBS three times and then mounted between a microscope slide and coverslip (Fisher Scientific). Fluorescence images were taken using Olympus BX61WI microscope with UPlanFL 40x 1.30 NA oil immersion objective lens and the FV300 Fluoview confocal laser-scanning microscope. For GAT-3 immunostaining experiments after electrophysiology, one astrocyte in each slice was pipette loaded with Alexa 488 fluorescent dye in the presence or absence of BAPTA within the intracellular solution. After loading for 20 min, the electrode was gently removed and the slice was fixed with 4% paraformaldehyde overnight followed by immunostaining as described above.

Data analysis and statistics

Image analysis was performed with ImageJ (NIH). All statistical tests were run in Origin 8 (OriginLab Corp). Data are as mean ± S.E.M from n experiments as indicated in the text, which was always greater than for 3 separate animals in each experiment for brain slice imaging and electrophysiology. Synaptic currents were analyzed using MiniAnalysis Program 6.0.7 (Synaptosoft). Two tailed *t* tests were used for most statistical analyses with significance declared at $p < 0.05$. The Kolmogorov–Smirnov two-sample test was used to compare cumulative probability curves of mIPSC amplitudes and mIPSC inter-event interval with significance declared at $p < 0.05$. Data are presented as mean ± s.e.m from *n* determination as shown in the text and figures.

Supplementary Material

Refer to Web version on PubMed Central for supplementary material.

Acknowledgments

The authors are indebted to Drs. TJ O'Dell and MV Sofroniew for discussions during the course of these experiments. The authors are grateful to Dr. E Toulme for assistance with Western blots, to Dr. M Hamby for tips on astrocyte enriched cultures and to Dr. S Kracun for molecular biology help and discussions. Thanks to Dr. M Nedergaard for discussions during the early stages of this project. Special thanks to members of the Astrocyte Biology and Biophysics Affinity Group at UCLA for discussions. Thanks to Dr. A Patapoutian (mTRPA1), Dr. D Julius (rTRPA1) and Dr. Y Gwack (mCherry) for sharing plasmids. Thanks to Dr. N Brecha for GAT-1 and GAT-3 antibodies. Our work was mainly supported by the NIH NINDS grant NS060677 and partly by grants NS071292 and NS063186, the Whitehall Foundation and a Stein-Oppenheimer Endowment Award (to BSK).

References

1. Halassa MM, Haydon PG. Integrated brain circuits: astrocytic networks modulate neuronal activity and behavior. Annu Rev Physiol. 2010; 72:335–355. [PubMed: 20148679]
2. Attwell D, et al. Glial and neuronal control of brain blood flow. Nature. 2010; 468:232–243. [PubMed: 21068832]
3. Henneberger C, Papouin T, Oliet SH, Rusakov DA. Long-term potentiation depends on release of D-serine from astrocytes. Nature. 2010; 463:232–236. [PubMed: 20075918]
4. Agulhon C, Fiacco TA, McCarthy KD. Hippocampal short- and long-term plasticity are not modulated by astrocyte Ca2+ signaling. Science. 2010; 327:1250–1254. [PubMed: 20203048]

5. Sontheimer H. Voltage-dependent ion channels in glial cells. Glia. 1994; 11:156–172. [PubMed: 7523291]
6. Bomben VC, Turner KL, Barclay TT, Sontheimer H. Transient receptor potential canonical channels are essential for chemotactic migration of human malignant gliomas. J Cell Physiol. 2011; 226:1879–1888. [PubMed: 21506118]
7. Hires SA, Tian L, Looger LL. Reporting neural activity with genetically encoded calcium indicators. Brain Cell Biol. 2008; 36:69–86. [PubMed: 18941901]
8. Tian L, et al. Imaging neural activity in worms, flies and mice with improved GCaMP calcium indicators. Nat Methods. 2009; 6:875–881. [PubMed: 19898485]
9. Shigetomi E, Kracun S, Khakh BS. Monitoring astrocyte calcium microdomains with improved membrane targeted GCaMP reporters. Neuron Glia Biology. 2010; 6:183–191. [PubMed: 21205365]
10. Shigetomi E, Kracun S, Sofroniew MV, Khakh BS. A genetically targeted optical sensor to monitor calcium signals in astrocyte processes. Nat Neurosci. 2010; 13:759–766. [PubMed: 20495558]
11. Halassa MM, Fellin T, Takano H, Dong JH, Haydon PG. Synaptic islands defined by the territory of a single astrocyte. J Neurosci. 2007; 27:6473–6477. [PubMed: 17567808]
12. Shigetomi E, Khakh BS. Measuring near plasma membrane and global intracellular calcium dynamics in astrocytes. J Vis Exp. 2009; 26
13. Clapham, DE. Transient Receptor Potential (TRP) Channels. In: Squire, LR., editor. Encyclopedia of Neuroscience. Vol. 9. Oxford: Academic Press; 2009. p. 1109-1133.
14. McNamara CR, et al. TRPA1 mediates formalin-induced pain. Proc Natl Acad Sci U S A. 2007; 104:13525–13530. [PubMed: 17686976]
15. Jordt SE, et al. Mustard oils and cannabinoids excite sensory nerve fibres through the TRP channel ANKTM1. Nature. 2004; 427:260–265. [PubMed: 14712238]
16. Bandell M, et al. Noxious cold ion channel TRPA1 is activated by pungent compounds and bradykinin. Neuron. 2004; 41:849–857. S0896627304001503 [pii]. [PubMed: 15046718]
17. Karashima Y, et al. Bimodal action of menthol on the transient receptor potential channel TRPA1. J Neurosci. 2007; 27:9874–9884. [PubMed: 17855602]
18. Cahoy JD, et al. A transcriptome database for astrocytes, neurons, and oligodendrocytes: a new resource for understanding brain development and function. J Neurosci. 2008; 28:264–278. [PubMed: 18171944]
19. Xiang Y, et al. Light-avoidance-mediating photoreceptors tile the Drosophila larval body wall. Nature. 2010; 468:921–926. [PubMed: 21068723]
20. García-Añoveros J, Nagata K. TRPA1. Handb Exp Pharmacol. 2007; 179:347–362. [PubMed: 17217068]
21. Wu LJ, Sweet TB, Clapham DE. International Union of Basic and Clinical Pharmacology. LXXVI. Current progress in the mammalian TRP ion channel family. Pharmacol Rev. 2010; 62:381–404. [PubMed: 20716668]
22. Reeves A, Shigetomi E, Khakh BS. Bulk loading of calcium indicator dyes to study astrocyte physiology: key limitations and improvements using morphological maps. J Neuroci. 2011; 31:9353–9358.
23. Kuchibhotla KV, Lattarulo CR, Hyman BT, Bacskai BJ. Synchronous hyperactivity and intercellular calcium waves in astrocytes in Alzheimer mice. Science. 2009; 323:1211–1215. [PubMed: 19251629]
24. Agulhon C, et al. What is the role of astrocyte calcium in neurophysiology? Neuron. 2008; 59:932–946. [PubMed: 18817732]
25. Kwan KY, et al. TRPA1 contributes to cold, mechanical, and chemical nociception but is not essential for hair-cell transduction. Neuron. 2006; 50:277–289. [PubMed: 16630838]
26. Soeller C, Cannell MB. Analysing cardiac excitation-contraction coupling with mathematical models of local control. Prog Biophys Mol Biol. 2004; 85:141–162. [PubMed: 15142741]
27. Gordon GR, et al. Astrocyte-mediated distributed plasticity at hypothalamic glutamate synapses. Neuron. 2009; 64:391–403. [PubMed: 19914187]

28. Overstreet LS, Jones MV, Westbrook GL. Slow desensitization regulates the availability of synaptic GABA(A) receptors. J Neurosci. 2000; 20:7914–7921. [PubMed: 11050111]
29. Glykys J, Mody I. Activation of GABAA receptors: views from outside the synaptic cleft. Neuron. 2007; 56:763–770. [PubMed: 18054854]
30. Lee S, et al. Channel-mediated tonic GABA release from glia. Science. 2010; 330:790–796. [PubMed: 20929730]
31. Ribak CE, Tong WM, Brecha NC. GABA plasma membrane transporters, GAT-1 and GAT-3, display different distributions in the rat hippocampus. J Comp Neurol. 1996; 367:595–606. [PubMed: 8731228]
32. Chiu CS, et al. Number, density, and surface/cytoplasmic distribution of GABA transporters at presynaptic structures of knock-in mice carrying GABA transporter subtype 1-green fluorescent protein fusions. J Neurosci. 2002; 22:10251–10266. [PubMed: 12451126]
33. Deken SL, Wang D, Quick MW. Plasma membrane GABA transporters reside on distinct vesicles and undergo rapid regulated recycling. J Neurosci. 2003; 23:1563–1568. [PubMed: 12629157]
34. Wang D, Quick MW. Trafficking of the plasma membrane gamma-aminobutyric acid transporter GAT1. Size and rates of an acutely recycling pool. J Biol Chem. 2005; 280:18703–18709. [PubMed: 15778221]
35. Macia E, et al. Dynasore, a cell-permeable inhibitor of dynamin. Dev Cell. 2006; 10:839–850. [PubMed: 16740485]
36. Shigetomi E, Bowser DN, Sofroniew MV, Khakh BS. Two forms of astrocyte calcium excitability have distinct effects on NMDA receptor-mediated slow inward currents in pyramidal neurons. J Neurosci. 2008; 28:6659–6663. [PubMed: 18579739]
37. Nilius B, Prenen J, Owsianik G. Irritating channels: the case of TRPA1. J Physiol. 2011; 589:1543–1549. [PubMed: 21078588]
38. Chen J, et al. Pore dilation occurs in TRPA1 but not in TRPM8 channels. Mol Pain. Jan 21.2009 5:3. [PubMed: 19159452]
39. Zurborg S, Yurgionas B, Jira JA, Caspani O, Heppenstall PA. Direct activation of the ion channel TRPA1 by Ca2+ Nat Neurosci. 2007; 10:277–279. [PubMed: 17259981]
40. Wang YY, Chang RB, Waters HN, McKemy DD, Liman ER. The nociceptor ion channel TRPA1 is potentiated and inactivated by permeating calcium ions. J Biol Chem. 2008; 283:32691–32703. [PubMed: 18775987]
41. Xu H, Delling M, Jun JC, Clapham DE. Oregano, thyme and clove-derived flavors and skin sensitizers activate specific TRP channels. Nat Neurosci. 2006; 9:628–635. [PubMed: 16617338]
42. Golovina VA. Visualization of localized store-operated calcium entry in mouse astrocytes. Close proximity to the endoplasmic reticulum. J Physiol. 2005; 564:737–749. [PubMed: 15731184]
43. Grimaldi M, Maratos M, Verma A. Transient receptor potential channel activation causes a novel form of [Ca 2+]I oscillations and is not involved in capacitative Ca 2+ entry in glial cells. J Neurosci. 2003; 23:4737–4745. 23/11/4737 [pii]. [PubMed: 12805313]
44. Malarkey EB, Ni Y, Parpura V. Ca2+ entry through TRPC1 channels contributes to intracellular Ca2+ dynamics and consequent glutamate release from rat astrocytes. Glia. 2008; 56:821–835. [PubMed: 18338793]
45. Shirakawa H, et al. Transient receptor potential canonical 3 (TRPC3) mediates thrombin-induced astrocyte activation and upregulates its own expression in cortical astrocytes. J Neurosci. 2010; 30:13116–13129. [PubMed: 20881130]
46. Everaerts W, et al. The capsaicin receptor TRPV1 is a crucial mediator of the noxious effects of mustard oil. Curr Biol. 2011; 21:316–321. [PubMed: 21315593]
47. Song I, Savtchenko L, Semyanov A. Tonic excitation or inhibition is set by GABA(A) conductance in hippocampal interneurons. Nat Commun. Jul 5.2011 2:376.10.1038/ncomms1377 [PubMed: 21730957]
48. Ortinski PI, et al. Selective induction of astrocytic gliosis generates deficits in neuronal inhibition. Nat Neurosci. 2010; 13:584–591. [PubMed: 20418874]
49. Moss FJ, et al. GABA transporter function, oligomerization state, and anchoring: correlates with subcellularly resolved FRET. J Gen Physiol. 2009; 134:489–521. [PubMed: 19948998]

50. Hill K, Schaefer M. Ultraviolet light and photosensitising agents activate TRPA1 via generation of oxidative stress. Cell Calcium. 2009; 45:155–164. [PubMed: 18814910]

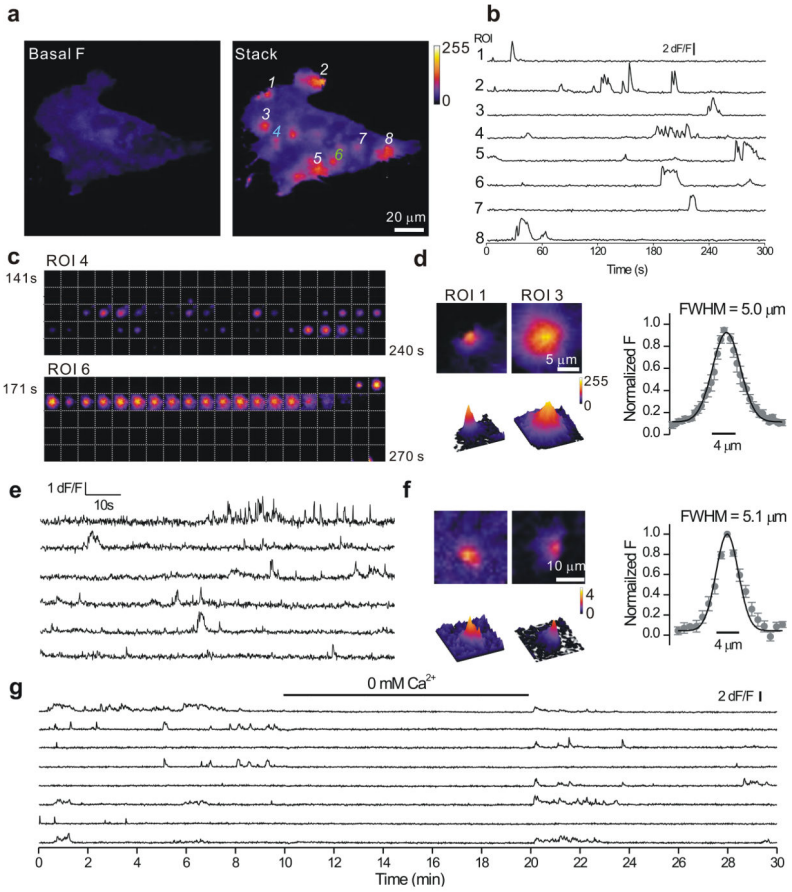

Figure 1. Spotty Ca^{2+} signals in rat hippocampal astrocyte-neuron co-cultures

a. Images of astrocytes expressing Lck-GCaMP3 in co-cultures. Left: basal fluorescence of Lck-GCaMP3 for an astrocyte before any spotty Ca^{2+} signals. Right: a maximum projection image of a 300 frame video. Eight regions of interest are shown (as 1–8). The intensity profiles of these eight ROIs are shown in **b. c.** Still frames between 141 and 240 s and between 171 and 270 s from the graph in panel **a** for ROI 4 and ROI 6. The time between images is 1 s. **d.** Images of spotty Ca^{2+} signals for ROI 1 and ROI 3. A graph on the right shows the full width of half maxima (FWHM) of the events (5.0 ± 0.6 μm, n = 10 sites). **e.** Intensity profiles of the six spotty Ca^{2+} signals observed by Fluo-4 Ca^{2+} indicator with total internal reflection fluorescence (TIRF) microscopy. **f.** Images of spotty Ca^{2+} signals visualized by TIRF microscopy. Spotty Ca^{2+} signals detected by TIRF occurred with a frequency of 1.8 events/min (n = 46 sites from 27 cells), lasted 0.6 ± 0.07 s (n = 408 events) and displayed peak dF/F values of ~100% (1.0 ± 0.03, n = 427). The graph on the right shows the FWHM of the events (5.1 ± 0.4 μm, n = 19 sites). **g**. Spotty Ca^{2+} signals imaged with Lck-GCaMP3 were reduced by ~95% in Ca^{2+} free conditions (Supplementary Video 2, n = 155 sites from 14 cells). Vertical lines are s.e.m.

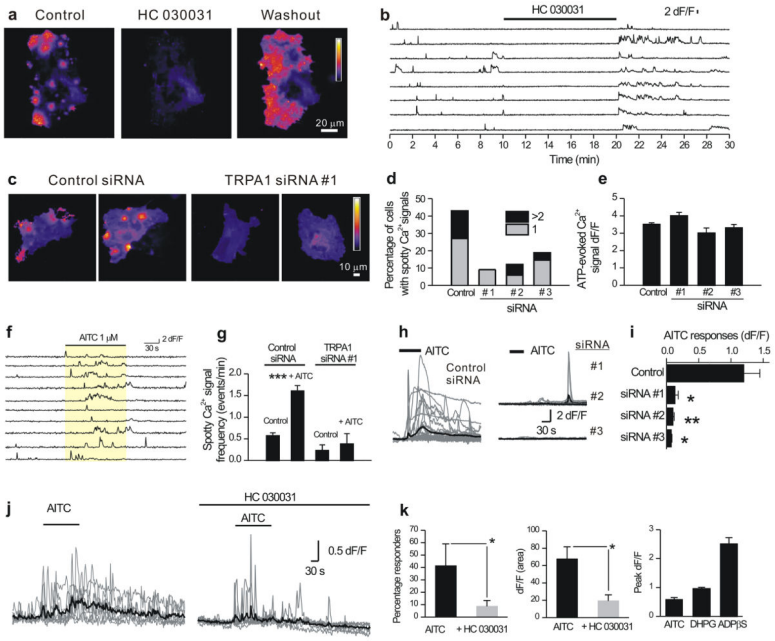

Figure 2. Evidence that TRPA1 channels mediate spotty Ca^{2+} signals in co-cultures

a. Maximum projections of a 300 frame video before (control), during and after (washout) of HC 030031 (40 μM). HC 030031 almost completely reduced spotty Ca^{2+} signals (Supplementary Video 3, from 0.49 ± 0.04 events/min to 0.025 ± 0.01 events/min by HC 030031; n = 96 sites from 11 cells, $p < 0.001$). **b.** Intensity versus time profile of eight ROIs. **c.** Maximal projection of 300 frame video with transfection of control siRNA (right panels, Supplementary Video 4) or TRPA1 siRNA #1 (left panels, Supplementary Video 5). **d.** Percentage of cells displaying spotty Ca^{2+} signals. TRPA1 siRNAs significantly ($p < 0.01$) reduced the number of astrocytes showing spotty Ca^{2+} signals (Fisher's exact test, control 43.6%, n=55 cells; siRNA#1, 9.1%, n=22 cells, $p = 0.0025$; siRNA#2, 12.1%, n = 33 cells, $p = 0.0014$; siRNA#3, 18.8%, n = 48 cells, p = 0.0052). **e.** Summary data of ATP-evoked Ca^{2+} signals measured with Lck-GCaMP3, in control conditions and when TRPA1 siRNAs were used. There was no significant change by TRPA1 siRNA transfection (control 3.5 ± 0.1, siRNA#1, 4.0 ± 0.2, p = 0.105; siRNA#2, 3.0 ± 0.3, p = 0.055; siRNA#3, 3.2 ± 0.2, p = 0.194). **f.** Numerous spotty Ca^{2+} signals were seen during the application of AITC (1 μM; Supplementary Video 6). AITC increased the frequency of spotty Ca^{2+} signals from 0.57 ± 0.07 to 1.6 ± 0.13 events min^{-1} ($p < 0.001$). **g.** Summary data on the frequency of spotty Ca^{2+} signals with or without AITC. With TRPA1 siRNA#1 transfection, AITC no longer increased the number of the events. **h.** AITC (20 μM)-induced global Ca^{2+} transients in astrocytes observed by Fluo-4. **i.** Average data showing that global Ca^{2+} signals evoked by AITC are blocked by siRNA against TRPA1. **j.** 100 μM AITC-evoked global Ca^{2+} increases measured in astrocytes in the stratum radiatum. The gray traces are representative single cells, whereas the black traces are the averages. **k.** Summary data for experiments such as those shown in panel **j**. The right hand bar graph plots the peak dF/F of the AITC-evoked responses (100 μM; n = 19) in relation to those evoked by DHPG (10 μM; n = 33) and ADPβS (30 μM; n = 21). Vertical lines are s.e.m.

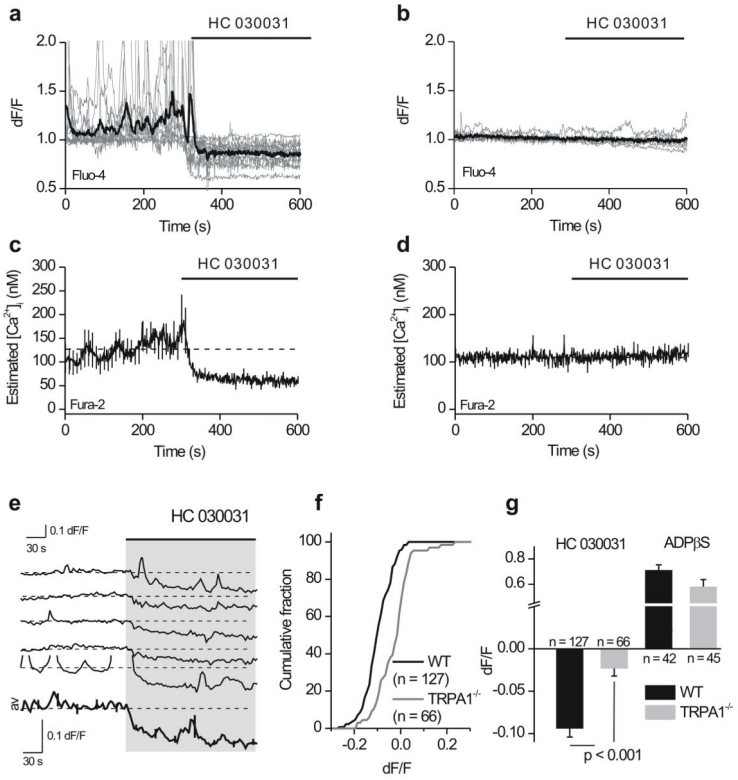

Figure 3. TRPA1 channels regulate basal Ca^{2+} levels in co-cultures and astrocytes in slices

a–b. Graphs plots dF/F over time from representative imaging experiments from astrocytes (a) and neurons (b) loaded with Fluo-4 (in co-cultures). For this comparison between neurons and astrocytes we studied both cells at 5–8 days in culture, when the neurons show less spontaneous activity than the astrocytes (compare panels **a** and **b**). **c–d.** Similar experiments to those shown in a–b, but for astrocytes (c) and neurons (d) loaded with Fura-2. The thick lines are an average from 10 and 7 cells for astrocytes and neurons, respectively. Note, with the use of Fura-2 the baseline is increasing for astrocytes but not neurons, possibly reflecting UV activation of TRPA1[50]. The dashed lines in panels c and d correspond to the mean level of Ca^{2+} before HC 030031. **e.** Experiments such as those in a, but for astrocytes loaded with Fluo-4 in acute hippocampal slices (Supplementary Fig. 9). **f.** A cumulative probability plot of dF/F evoked by HC 030031 applications to astrocytes in acute hippocampal slices from wild type and *TRPA1*$^{-/-}$ mice. **g.** Bar graph showing that the ability of HC 030031 to reduce resting Ca^{2+} levels in astrocytes from *TRPA1*$^{-/-}$ mice is almost completely abolished. Astrocytes from wild type and *TRPA1*$^{-/-}$ mice responded equally well to ADPβS (30 μM). Vertical lines are s.e.m.

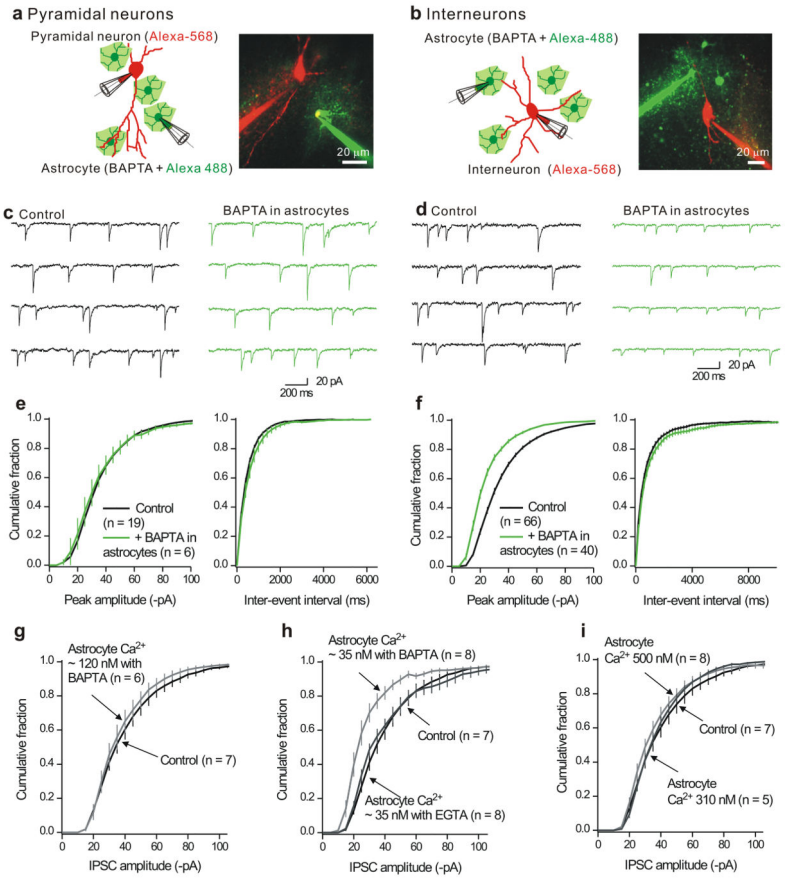

Figure 4. Buffering astrocyte intracellular Ca^{2+} levels decreases mIPSC amplitudes in interneurons, but not pyramidal neurons in hippocampal slices

a. The left cartoon shows the protocol whereas the image shows a representative confocal image. The astrocytes were loaded with Alexa-488 (100 μM) whereas the neurons were loaded with Alexa-568 (100 μM). Recordings were made from neurons and astrocytes that were no more than 100 μm apart. In this approach, we recorded from a population of neurons, determined mIPSC parameters and then record from a second population in which the astrocyte nearby had also been patched. **b**. As in a, but for dual recordings from astrocytes and interneurons in the stratum radiatum region. **c**. Representative mIPSCs recorded from CA1 pyramidal neurons under controls settings, and also for pyramidal neurons located near astrocytes that were dialyzed with 13 mM BAPTA (>20 min). **d**. As in c, but for whole-cell recording from interneurons. **e**. Cumulative probability plots of pyramidal neuron mIPSC amplitudes and inter-event intervals from control neurons and those located near astrocytes dialyzed with BAPTA. **f**. As in e, but for mIPSCs recorded from interneurons. **g–h**. Average cumulative probability plots for interneurons located near astrocytes dialyzed with intracellular solutions to clamp the bulk concentration of Ca^{2+} ions to known levels using either the fast chelator BAPTA, or the slower chelator EGTA. No significant changes were observed for the inter-event interval distributions (Supplementary Fig. 11). In this and all subsequent figures, the vertical lines on the cumulative probability plots represent the standard error of the mean (s.e.m).

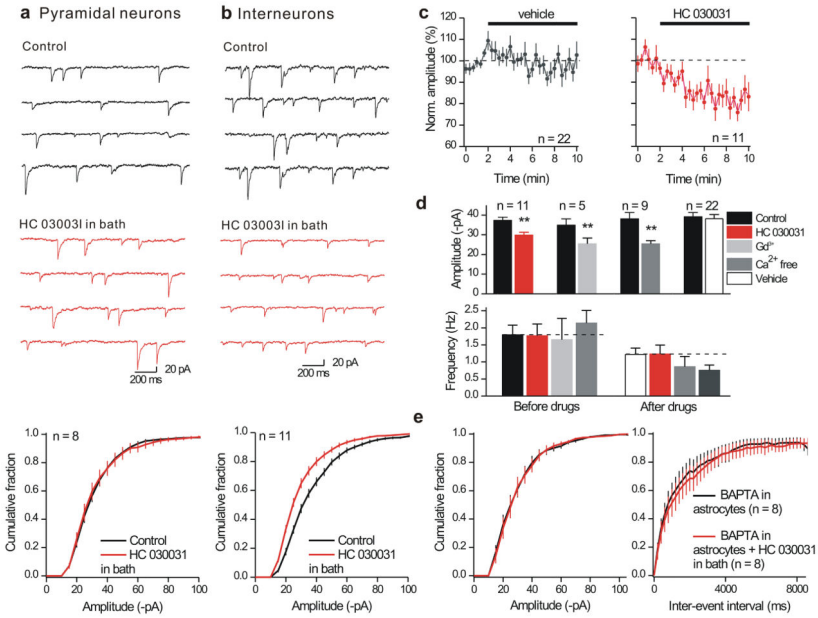

Figure 5. Effect of the TRPA1 channel blocker (HC 030031) on mIPSCs arriving onto pyramidal neurons and interneurons in the hippocampus

a. Representative traces for mIPSCs recorded from CA1 pyramidal neurons before and during bath applications of HC 030031 (40 μM) for 8 minutes. The traces and the average cumulative probability plot below shows that HC 030031 produced no effect on mIPSC amplitudes (frequency was also not affected: reported in the text). **b**. As in a, but for recordings from interneurons. **c**. Plots the normalized mIPSC amplitude over time for cells where HC 030031 was applied for the duration indicated by the solid black bar in relation to cells where vehicle (0.1% DMSO) was applied. **d**. Summarizes average mIPSC amplitude and frequency data recorded from interneurons under the indicated conditions. **e**. HC 030031 did not alter mIPSC amplitudes when astrocytes were previously dialyzed with BAPTA. The parallel control experiments with BAPTA are shown in Supplementary Fig. 13a,b. Vertical lines are s.e.m.

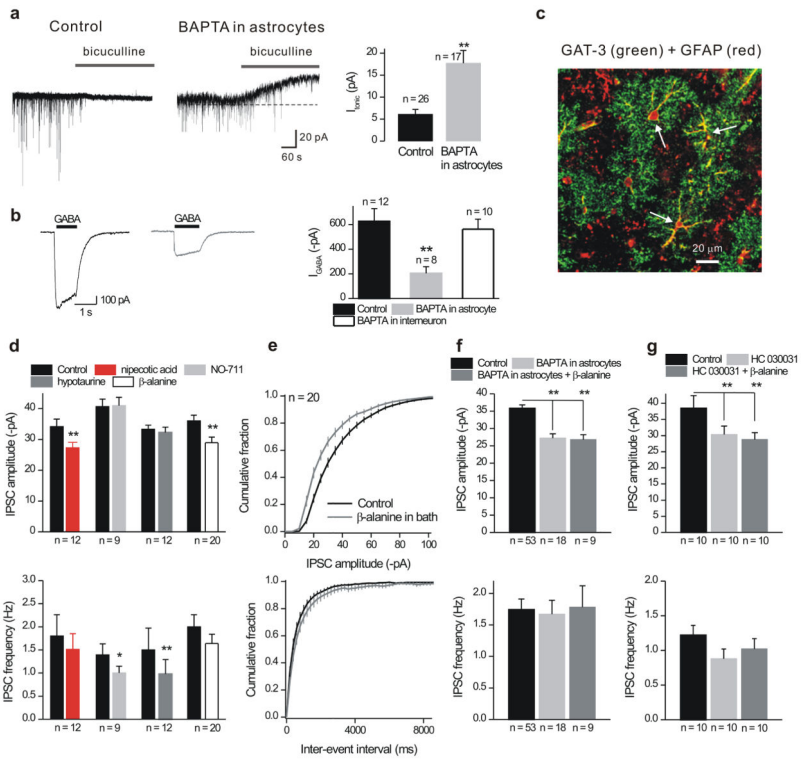

Figure 6. Role of GAT-3 GABA transporters

a. The upper traces show the effect of bicuculline (50 μM) applications on holding current (at −60 mV) measured from interneurons under control settings, or from interneurons located within 100 μm of astrocytes dialyzed with BAPTA for 20 mins (right). The bar graph summarizes the findings. We did not measure reversal upon bicuculline washout as this was incomplete by 30 mins. **b.** Representative traces for currents evoked by puff application of GABA (30 μM) in control conditions and after 20–25 mins of astrocyte dialysis with BAPTA (the traces are from different cells). The bar graph summarizes the findings. **c.** The confocal images show GAT-3 and GFAP staining in stratum radiatum (Supplementary Fig. 14). **d.** Summary data for mIPSC amplitudes (upper graph) and frequency (lower graph) when all GABA transporters were blocked (nipecotic acid; 100 μM), when GAT-1 was blocked (NO-711; 10 μM), when GAT-2 was blocked (hypotaurine; 100 μM) and when GAT-3 was blocked with β-alanine (100 μM). **e.** Average cumulative probability plots of mIPSC amplitude and inter-event interval distributions under control settings and after blockade of GAT-3 with β-alanine (100 μM). **f.** The bar graphs summarize the finding that astrocyte dialysis with BAPTA (13 mM) occluded the effect of β-alanine on mIPSC amplitudes (upper panel). The mIPSC frequency was not affected. **g.** As in c, but in this case prior application of HC 030031 (40 μM) occluded the effect of β-alanine on mIPSC amplitudes. mIPSC frequency was unaffected. In these graphs ** indicated $p < 0.01$ by an unpaired Students *t* test. Vertical lines are s.e.m.

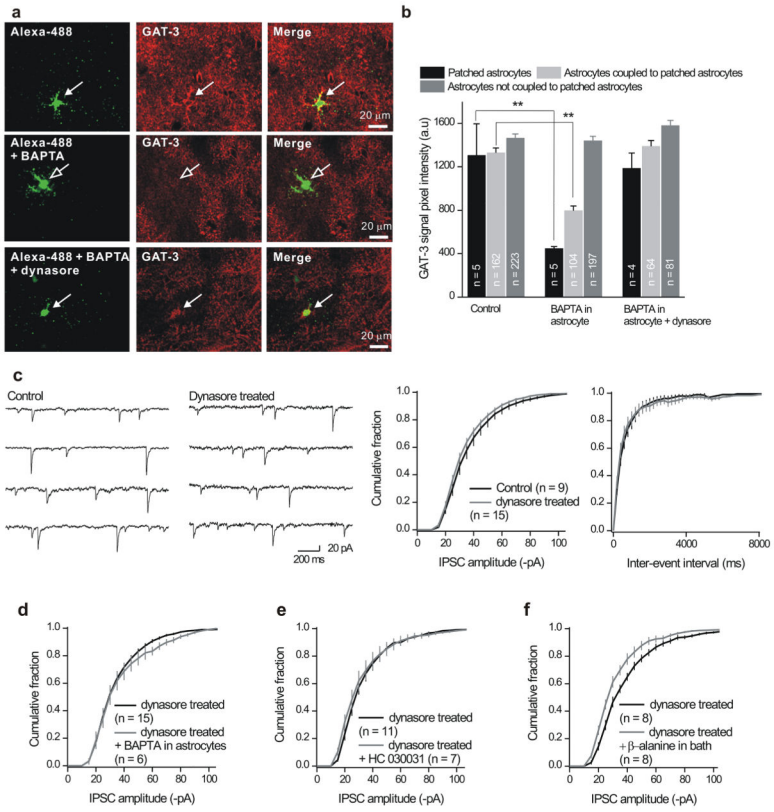

Figure 7. Astrocyte dialysis with BAPTA regulates GAT-3 in astrocytes

a. The upper panels show images of an astrocyte in the stratum radiatum. The astrocyte had been dialyzed with Alexa-488 and then processed for GAT-3 staining. The middle panels show images for similar experiments when the astrocyte had been dialyzed with Alexa-488 and BAPTA (13 mM). In this case the colocalisation between Alexa-488 and GAT-3 was reduced because there was less GAT-3 immunostaining in the patched astrocyte. The lower panels show images for slices pretreated with dynasore. **b.** Summarizes data from experiments such as those shown in panel a. **c.** Representative traces and cumulative probability plots show that dynasore (100 μM) did not affect mIPSC amplitude or inter-event interval distributions during recordings from interneurons. **d.** Dynasore pretreatment abolished the ability of astrocyte BAPTA dialysis to reduce mIPSC amplitudes onto interneurons. **e.** Dynasore pretreatment also abolished the ability of HC 030031 to reduce the mIPSC amplitudes. **f.** Dynasore pretreatment did not affect the ability of β-alanine (GAT-3 blocker) to reduce the amplitude of mIPSCs onto interneurons. For panels d–f, the mIPSC frequencies are presented in the text (they were not altered). The scale bar for the images is 20 μm (in panel a). Vertical lines are s.e.m.

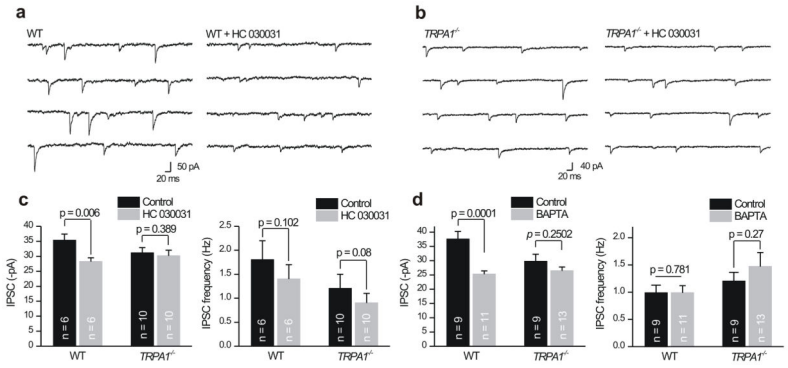

Figure 8. The effects of HC 030031 and astrocyte BAPTA dialysis are abolished in the *TRPA1*$^{-/-}$ mice

a. Representative traces for interneuron mIPSCs recorded from wild type control mice before and during HC 030031 applications (40 μM). The mIPSCs were reduced in amplitude as shown in earlier parts of this study. **b.** As in a, but for recordings from *TRPA1*$^{-/-}$ mice. In this case HC 030031 was without effect. **c.** Summary data for mIPSC amplitudes from *TRPA1*$^{-/-}$ and wild type controls for experiments such as those shown in panels a and b. **d.** Summary data for mIPSC amplitudes from *TRPA1*$^{-/-}$ and wild type controls for experiments where astrocytes were dialyzed with BAPTA. Vertical lines are s.e.m.